

The problem of the critical angle for edge and center V-notched structures

Original

The problem of the critical angle for edge and center V-notched structures / Carpinteri, Alberto; Cornetti, Pietro; Pugno, Nicola; Sapora, ALBERTO GIUSEPPE. - (2010). (ECF 18 Dresda (Germany) 30 agosto - 3 settembre 2010).

Availability:

This version is available at: 11583/2499411 since: 2016-05-11T11:47:38Z

Publisher:

Aedificatio Publishing

Published

DOI:

Terms of use:

This article is made available under terms and conditions as specified in the corresponding bibliographic description in the repository

Publisher copyright

(Article begins on next page)

THE PROBLEM OF THE CRITICAL ANGLE FOR EDGE AND CENTER V-NOTCHED STRUCTURES

A. Carpinteri¹⁾, P. Cornetti¹⁾, N. Pugno¹⁾, A. Saporà¹⁾

¹⁾Politecnico di Torino, Department of Structural Engineering and Geotechnics,
Corso Duca degli Abruzzi 24, 10129 Torino, Italy

ABSTRACT

In the present paper, the problem of detecting the critical notch angle, i.e. the angle providing the minimum failure load, for brittle or quasi-brittle structures containing either edge or center V-notches is investigated. The expression of the generalized fracture toughness is obtained according to Finite Fracture Mechanics. It is shown that a critical angle is always present: its value depends, through the brittleness number, on both material and geometric characteristics. Thus, the crack is not the most dangerous configuration. The result is supported by experimental results presented in the Literature.

KEYWORDS

Edge and center V-notched structures, Notch sensitivity, Finite Fracture Mechanics

INTRODUCTION

Many experimental results [1-4] concerning three-point bending (TPB) and tensile tests on V-notched brittle or quasi-brittle material specimens, show that the failure load does not increase monotonically as the notch opening angle ω increases, but it has a minimum in correspondence of a critical angle ω_c . The problem of determining ω_c was investigated in [5] to what concerns a semi-infinite edge V-notched slab and it is here extended to a center V-notched infinite slab under remote tensile load, when the notch is subjected to mode I loading. Four different criteria based on a discrete crack advancement [2,6-8] are taken into account. Despite their predictions slightly differ from each other, all the approaches detect the minimum, whose value depends on the brittleness number s [9]: the larger s (i.e. the larger the fracture toughness and/or the smaller the tensile strength and/or the smaller the notch depth), the larger the ω_c expected. A final comparison between theoretical predictions and experimental data confirms the validity of the present analysis.

ANALYSIS OF SEMI-INFINITE EDGE AND CENTER V-NOTCHED SLABS

The generalized stress intensity factor (SIF) K_I^* related to an edge semi-infinite V-notched slab or to a center V-notched infinite slab under remote tensile load σ (Fig. 1) can be expressed, by means of dimensional analysis, as [1]:

$$K_I^* = \beta(\omega) \sigma a^{1-\lambda(\omega)}, \quad (1)$$

where a is the notch depth for the edge notch case and half of its length in the centre notch case, λ is the solution of the eigen-equation derived by Williams (1952) and β is the shape function, which depends only on the notch angle ω . Values of β related to the two considered geometries can be found tabulated in [10] and they are plotted in Fig. 2 (note that they are modified according to the different definition of the generalized stress-intensity factor here

adopted i.e., $\sigma_y(x) = K_I^* / (2\pi x)^{1-\lambda}$ instead of $\sigma_y(x) = K_I^* / x^{1-\lambda}$, xy being the reference system centred at the V-notch tip (Fig. 1)). They differ by a factor 1.12 for $\omega=0^\circ$, while they coincide for $\omega=180^\circ$.

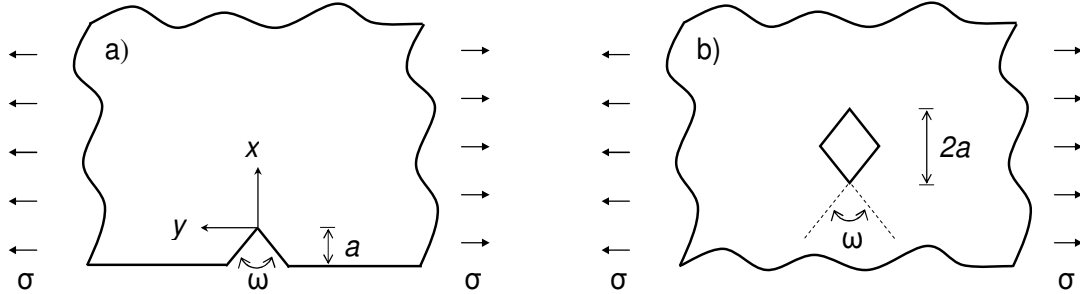


Fig. 1: Geometry of tensile slabs: a) semi-infinite edge-notched b) infinite center-notched.

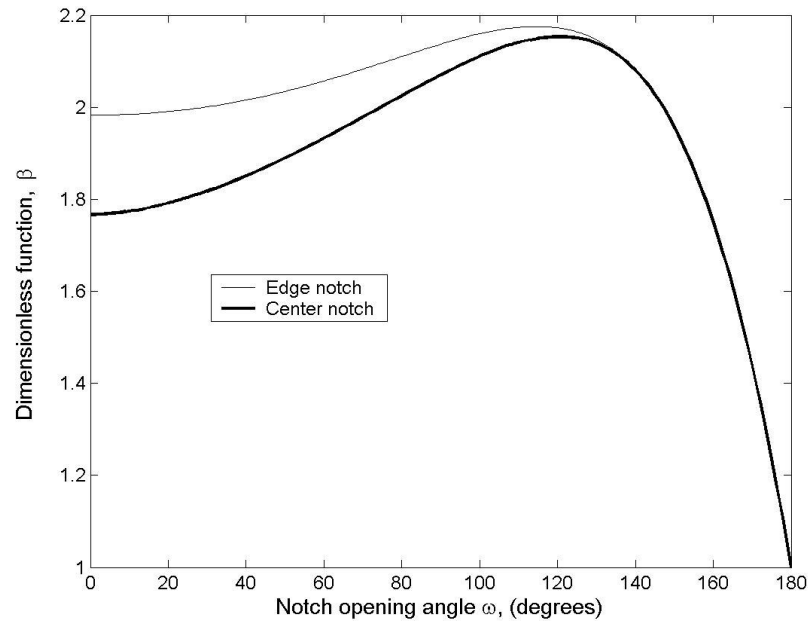


Fig. 2: Function β for a semi-infinite edge notched slab (thin line) and for an infinite center-notched slab (thick line) under remote tensile load.

The generalized SIF K_I^* is the coefficient of the dominant term of the stress field at the notch tip and, within brittle structural behaviour, it is expected to be the governing failure parameter. In other words, failure is supposed to take place whenever [1]:

$$K_I^* = K_{Ic}^*, \quad (2)$$

K_{Ic}^* being the generalized fracture toughness. A theoretical justification of this fracture criterion (Eq. 2) may be given in the framework of Finite Fracture Mechanics (FFM). According to FFM, fracture does not propagate continuously but by finite crack extensions Δ , leading to the following general relationship

$$K_{lc}^* = \xi(\omega) \frac{K_{lc}^{2(1-\lambda)}}{\sigma_u^{1-2\lambda}}, \quad (3)$$

where $\xi(\omega)$ is a dimensionless function depending on the fracture criterion used, while K_{lc} and σ_u are the fracture toughness and tensile strength, respectively.

Different $\xi(\omega)$ functions and critical distances Δ related to different FFM approaches, are summarized in Table 1: they refer to the average stress (LS) criterion [2], the average energy (LE) criterion [6], the coupled point stress and average energy (PSLE) criterion [7], and the coupled average stress and average energy (LSLE) criterion [8].

The energy-based criteria all involve a dimensionless coefficient μ , depending on the notch angle ω , which rises from the evaluation of the SIF for a short crack at the V-notch [11]. μ values can be found tabulated either in [12] or, in the present notation, in [5]. It increases from unity, when $\omega=0^\circ$, up to $1.12\sqrt{\pi}$, when $\omega=180^\circ$. On the other hand, the constant c assumes only two values: 1 for the center-crack case and 1.12 for the edge-crack case.

Criterion	LS	LE	PSLE	LSLE
$\xi(\omega)$	$\lambda 4^{1-\lambda}$	$\frac{c\sqrt{\pi\lambda}}{\mu} \left(\frac{2}{\pi c^2} \right)^{1-\lambda}$	$\lambda^{1-\lambda} \left[\frac{(2\pi)^{2\lambda-1}}{\mu^2/2} \right]^{1-\lambda}$	$\lambda^\lambda \left[\frac{(2\pi)^{2\lambda-1}}{\mu^2/2} \right]^{1-\lambda}$
Δ	$\frac{2}{\pi} \left(\frac{K_{lc}}{\sigma_u} \right)^2$	$\frac{2}{\pi c} \left(\frac{K_{lc}}{\sigma_u} \right)^2$	$\frac{2\lambda}{\mu^2 (2\pi)^{2(1-\lambda)}} \left(\frac{K_{lc}}{\sigma_u} \right)^2$	$\frac{2}{\lambda \mu^2 (2\pi)^{2(1-\lambda)}} \left(\frac{K_{lc}}{\sigma_u} \right)^2$

Table 1: Different ξ functions and critical distances Δ according to different FFM criteria.

Observe that the critical distances related to the coupled criteria are structural parameters, depending, through λ and μ , also on the notch opening angle ω .

Inserting Eqs. (1) and (3) into Eq. (2), yields:

$$\frac{\sigma_f}{\sigma_u} = \frac{\xi}{\beta} \alpha^{\lambda-1}, \quad (4)$$

where σ_f is the remote stress at failure and α is the dimensionless notch depth

$$\alpha = \frac{1}{s^2} = a \left(\frac{\sigma_u}{K_{lc}} \right)^2. \quad (5)$$

The brittleness number s was introduced by Carpinteri [8]: low brittleness numbers correspond to brittle structural behaviours. In the present case, i.e. infinite or semi-infinite slabs, the characteristic structural size a is proportional to the notch depth, the only relevant size in the problem.

NOTCH SENSITIVITY

The determination of the critical notch angle may be formalized by deriving Eq. (4) with respect to ω and imposing the stationary condition. The following relationship is hence obtained:

$$\alpha = \exp \left[\frac{1}{\lambda'} \left(\frac{\beta'}{\beta} - \frac{\xi'}{\xi} \right) \right] \bigg|_{\omega = \omega_c} \quad (6)$$

By evaluating the derivatives λ' , β' and ξ' with respect to the notch opening angle ω , the inverse of Eq. (6) is plotted in Figs. 3 and 4, for the two geometries considered, providing the value of the critical notch opening angle ω_c for a given α (or s) value. As it can be observed, in both the cases, ω_c depends through s both on the material and the geometry. It is evident that the crack is the most dangerous V-notch ($\omega_c=0^\circ$) only for extremely large notches and/or very brittle material (i.e., high fracture toughness and/or small tensile strength). All the FFM criteria are able to catch the minimum, although their predictions slightly differ from each other. Particularly, the PSLE approach generally provides the lowest ω_c values, while the highest ω_c values are obtained through the LSLE criterion.

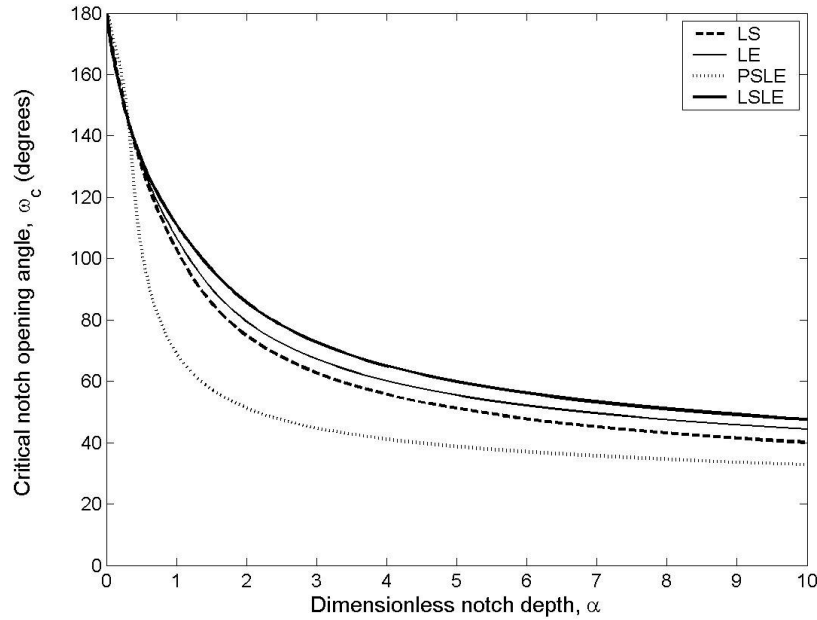


Fig. 3: Semi-infinite edge-notched slab under remote tensile load: critical notch-opening angle ω_c vs. dimensionless notch depth α according to different FFM criteria.

The problem could also be analyzed from the opposite point of view, that is by varying α (i.e., s), and keeping ω fixed in Eq. (4). For the sake of clarity, only the results obtained by applying the LSLE approach to the semi-infinite edge-notched slab are plotted in Fig. 5. It is evident that the minimum failure load is provided by the edge crack case only for $\alpha \rightarrow \infty$ ($s \rightarrow 0$), whereas it corresponds to the flat edge for $\alpha \rightarrow 0$ ($s \rightarrow \infty$). In the intermediate cases, the minimum failure load is provided by a V-notch of amplitude ω_c ranging from 0° up to 180° as α decreases from infinite to zero. In Fig. 5 also the envelope has been drawn, i.e. the line that is tangent to all the diagrams plotted keeping ω fixed, which provides the minimum achievable relative failure stress for each relative notch depth α . The graphic related to the center-notch case is very similar, as, qualitatively, those obtained by the other FFM criteria.

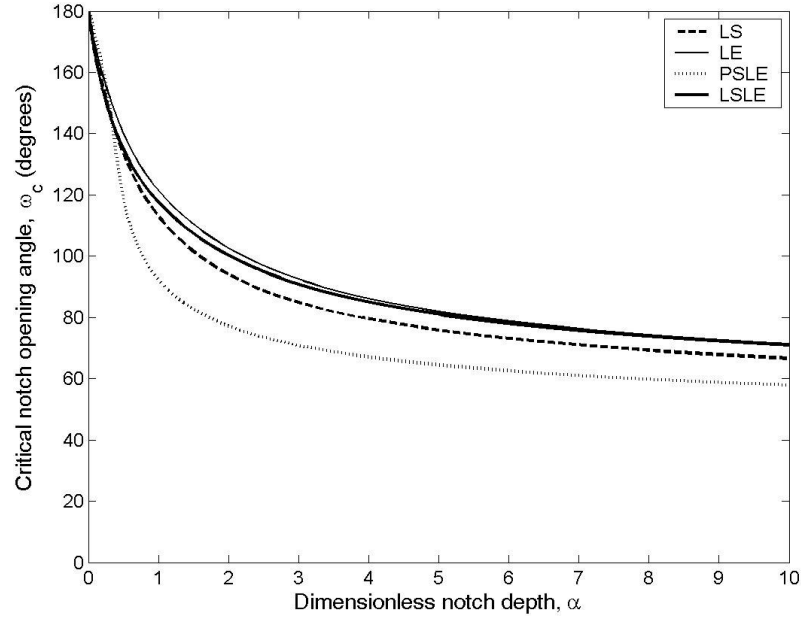


Fig. 4: Infinite center-notched slab under remote tensile load: critical notch-opening angle ω_c vs. dimensionless notch depth α according to different FFM criteria.

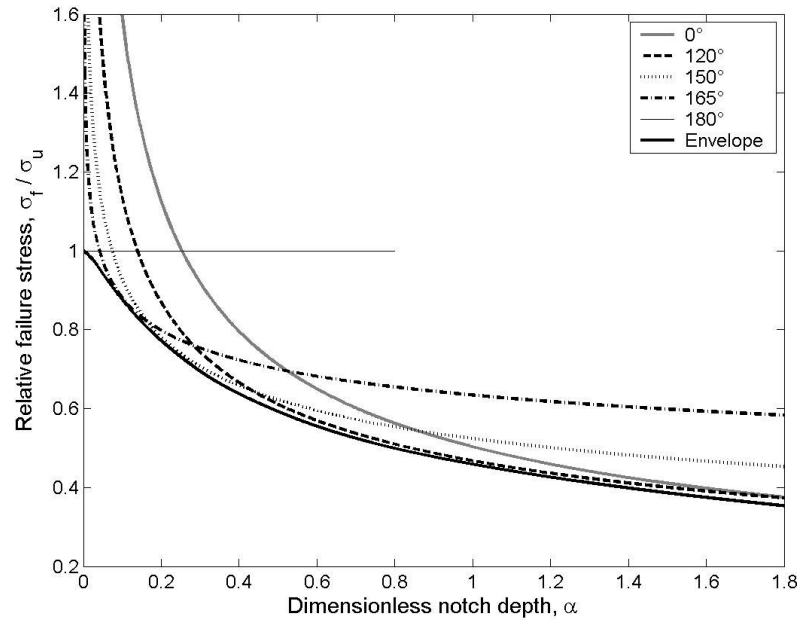


Fig. 5: Dimensionless failure load vs. dimensionless notch depth for a semi-infinite edge-notched slab, according to the LSLE criterion. The black thick line represents the envelope of the other curves.

COMPARISON WITH EXPERIMENTAL DATA

A comparison between experiments and theoretical predictions, provided by different FFM criteria, is performed in this section. In the case of finite geometries, notice that, by means of dimensional analysis, Eq. (4) can be rewritten as:

$$\frac{P_{cr}^{\omega}}{P_{cr}^{\pi}} = \frac{\xi(\omega)}{f(a/h, l/h, \omega)} s^{2(1-\lambda)} \quad (7)$$

where P_{cr}^{ω} and P_{cr}^{π} are the failure loads for a notch opening angle equal to ω and 180° , respectively, h is the specimen height and l its length. The shape function f replacing β , depends now not only on the amplitude but also on the relative notch depth and the slenderness ratio. Indeed, this latter dependence is practically negligible for tensile specimens with $l/h > 2$ and for TPB specimens with $l/h > 8$. The brittleness number now recovers the usual expression $s = K_{Ic}/(\sigma_u \sqrt{h})$.

All the experimental data here considered [1-4] share the following common features:

- The samples are edge V-notched: the notch radius is small enough not to affect the results. Moreover, specimens referring to TPB tests show a slenderness ratio $l/h \approx 4$, while, for tensile tests, $l/h > 2$.
- The loading is applied in mode I and fracture is of a brittle character.
- The presence of a critical angle ω_c rises from the evaluated failure loads, which do not increase strictly monotonically as a function of the notch opening angle ω .

TPB tests on V-notched PMMA specimens carried out by Carpinteri [1], for instance, show the minimum failure load for $\omega_c \sim 45^\circ$ (Fig. 6a). Similar results ($\omega_c \sim 40^\circ$) are obtained by Seweryn [2], testing double-edge notched tension (DENT) PMMA samples (Fig. 6b). Strandberg [3] performed tests on single edge notched tension (SENT) specimens made of soft annealed tool steel at -50°C . Although, in this case, the cracked specimens are the ones providing the minimum failure load, this lowest value, according to the Author himself, is due to pre-cracking procedure carried out to manufacture the cracked specimen and to a crack depth deviating by +16% from that related to the other tested geometries. For this reason, the fracture toughness value (as well as that of the tensile strength) were obtained from a best fit procedure in [3]. The same will obviously apply in the present study (Table 2). Moreover, since the failure load slightly decreases by passing from 30° to 60° and afterwards it increases monotonically with ω , $\omega \sim 60^\circ$ can be regarded as a minimum (Fig. 6c). Eventually, TPB tests carried out on polystyrene specimens [4] do not show a significant difference between the failure load for 60° -notch sample and 120° -notch sample (Fig. 6d) and the presence of a minimum between these two cases can be argued.

In Fig. 6 there are also reported FFM predictions by means of Eq. 7. Shape functions are obtained either numerically [13] or by exploiting those already evaluated, as done for steel samples [3]: in this case, however, the shape function related to the crack-case has been recalculated. Material and structural properties, to what concerns different experiments, are reported in Table 2.

As it can be seen from Fig. 6, a good agreement is generally found between experimental data and theoretical predictions. The highest values for the relative failure loads are provided by the PSLE criterion: its predictions slightly differ from those obtained by the other FFM criteria, which result to be very close. Notice that the LSLE approach always provides the lowest values. These behaviours also reflect on the critical angle ω_c value, which is caught by all the FFM criteria (Table 2). For smaller s , the minimum is less marked (Fig. 6) and similar results are obtained from different approaches: while for DENT PMMA samples the critical value approaches the experimental one, for TPB PMMA specimens is lower. Note anyway,

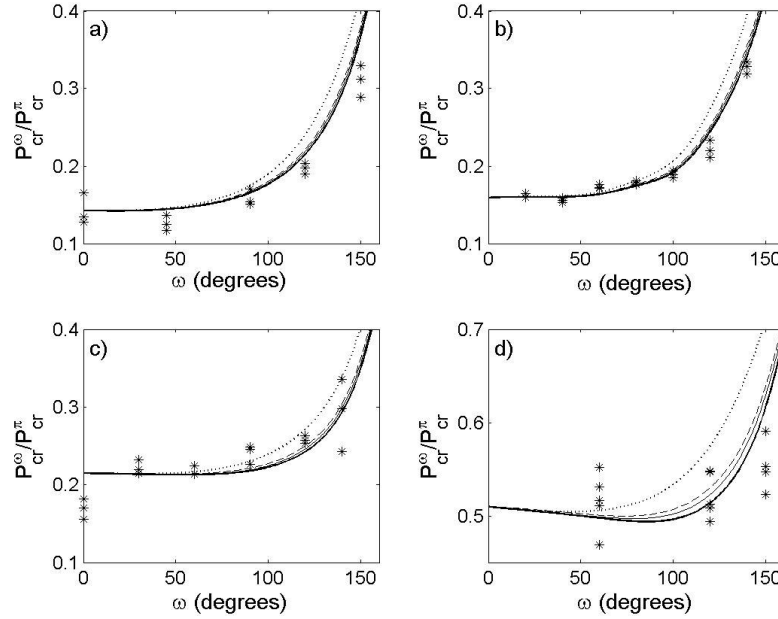


Fig. 6: Relative failure loads vs. notch opening angle for different experimental tests: a) TPB, PMMA [1], b) DENT, PMMA [2], c) SENT, steel [3], d) TPB, polystyrene [4]. Experimental data (asterisks) and predictions related to different FFM criteria: LS (dashed line), LE (continuous thin line), PSLE (dotted line) and LSLE (continuous thick line).

that no specimens with notch amplitude comprised between 0° and 45° were tested in [1]. For higher s (steel and polystyrene), the scattering between the predictions of the ω_c value is slightly higher, especially for the PSLE criterion. Eventually, observe from Table 2 that the LSLE predictions on the critical angle result to be the closest to the experimental values and that the general trend obtained in Fig. 3 (i.e., the semi-infinite edge-notched geometry) is coherently recovered.

Tests	TPB, PMMA	DENT, PMMA	SENT, steel	TPB, polystyrene
σ_u (MPa)	123.80	104.90	2006.00	70.61
K_{Ic} (MPa \sqrt{m})	1.92	1.86	58.24	2.23
s	0.0693	0.0756	0.1676	0.2354
ω_c (exp.)	$\sim 45^\circ$	$\sim 40^\circ$	$\sim 60^\circ$	-
ω_c (LS)	24°	30°	48°	75°
ω_c (LE)	25°	32°	49°	80°
ω_c (PSLE)	21°	24°	32°	45°
ω_c (LSLE)	25°	34°	54°	87°

Table 2: Material properties related to the experimental data considered in the present analysis and critical angle values ω_c obtained experimentally and through different FFM criteria.

CONCLUSIONS

The presence of a critical angle providing the minimum failure load, in brittle or quasi-brittle structures containing edge and center re-entrant corners, is investigated. The study concerns both infinite and finite geometries, under different loading conditions. It is shown that a critical

angle always exists and is more pronounced for large s values (i.e. relatively ductile materials and/or small structural sizes), while it becomes almost imperceptible for small s values: only in this case the crack tends to become the most dangerous configuration.

Acknowledgments The financial support of the Italian Ministry of Education, University and Research (MIUR) to the Project “Advanced applications of Fracture Mechanics for the study of integrity and durability of materials and structures” within the PRIN program for the year 2008 is acknowledged.

REFERENCES

- [1] Carpinteri, A.:
Stress-singularity and generalized fracture toughness at the vertex of re-entrant corners
Eng Fract Mech 26 (1987), 143-155.
- [2] Seweryn, A.:
Brittle fracture criterion for structures with sharp notches
Eng Fract Mech 47 (1994), 673-681.
- [3] Strandberg, M.:
Fracture at V-notches with contained plasticity
Eng Fract Mech 69 (2002), 403-415.
- [4] Carpinteri, A.; Cornetti, P.; Pugno, N.; Sapora, A.; Taylor, D.:
A finite fracture mechanics approach to structures with sharp V-notches
Eng Fract Mech 75 (2008), 1736-1752.
- [5] Carpinteri, A.; Cornetti, P.; Pugno, N.; Sapora, A.:
On the most dangerous V-notch
Int J Solids Struct 47 (2010), 887–893
- [6] Pugno, N.; Ruoff, R.:
Quantized fracture mechanics
Philos Mag 84 (2004), 2829-2845.
- [7] Leguillon, D.:
Strength or toughness? A criterion for crack onset at a notch
Eur J Mech A/Solids 21 (2002), 61-72
- [8] Cornetti, P.; Pugno, N.; Carpinteri, A.; Taylor, D.:
Finite fracture mechanics: a coupled stress and energy failure criterion
Eng Fract Mech 73 (2006), 2021–2033.
- [9] Carpinteri, A.:
Notch sensitivity in fracture testing of aggregative materials
Eng Fract Mech 16 (1982), 467-481
- [10] Dunn, M.; Suwito, W.; Cunningham, S.:
Stress intensities at notch singularities
Eng Fract Mech 57 (1997), 417-430.
- [11] Hasebe, N.; Iida, J.:
A crack originating from a triangular notch on a rim of a semi-infinite plate
Eng Fract Mech 10 (1978), 773-782.
- [12] Philipps, A.G.; Karuppanan, S.; Churchman, C.M; Hills, D.D.:
Crack tip stress intensity factors for a crack emanating from a sharp notch
Eng Fract Mech 75 (2008), 5134-5139
- [13] Carpinteri, A.; Cornetti, P.; Pugno, N.; Sapora, A.; Taylor, D.:
Generalized fracture toughness for specimens with re-entrant corners: experiments vs. theoretical predictions
Struct Eng Mech 32 (2009), 609–620.

Corresponding author: alberto.sapora@polito.it